Iranian Journal of Chemical Engineering
Vol. 7, No. 3 (Summer), 2010, IAChE

Investigation of CO Injection Effect on the Methanol Production in a Single Type Reactor in the Presence of Catalyst Deactivation

F. Rahmani[1], M. Bayat[1], M. Haghighi[2], M. R. Rahimpour[1]*

1- Chemical Engineering Department, School of Chemical and Petroleum Engineering, Shiraz University, Shiraz, Iran
2- Reactor and Catalysis Research Center (RCRC), Chemical Engineering Department, Sahand University of Technology, Sahand New Town, Tabriz, Iran

Abstract

In this work, the behavior of a single-type industrial methanol reactor while the 5% CO was injected into the 95% of feed was investigated. For the dynamic simulation purposed, a heterogeneous one-dimensional model has been developed in the presence of long term catalyst deactivation. The performance of the reactor with CO injection to the feed entrance was investigated and the product and reactant mole fraction profiles of the aforesaid reactor were compared with that of a conventional single type (CMR) and membrane methanol reactor (MMR). The simulation results represent 14.24% and 22.93% enhancement in the yield of methanol production in comparison with MMR and CMR, respectively, while 5% CO was injected into the 95% of the feed. Also, by CO injection to the feed, water production during methanol synthesis via CO_2 hydrogenation which accelerates the catalyst deactivation and reduces methanol production rate, is reduced greatly. Additionally, nowadays CO is an important cause of pollution and a hazardous material in many industrial processes and using it in these processes is one of the ways to solve the pollution problem.

Keywords: *Dynamic Simulation, Single-type Reactor, Methanol Production, CO Injection*

1- Introduction

Methanol is an important industrial chemical that will play a major role in the energy sector, where it could provide a convenient hydrogen source for fuel cells, or serve as an intermediate for synthetic fuels such as dimethyl ether (DME) [1] and as a raw material for the production of chemicals such as formaldehyde and acetic acid. Methanol synthesis is the second largest present use of hydrogen after ammonia synthesis, and is produced by the catalytic conversion of synthesis gas (H_2, CO_2, CO) [2]. Improvement in the production efficiency of important chemicals by only a few percent can sometimes result in significant profit increase, energy conservation and environmental protection, especially for a chemical such as methanol which is produced in a worldwide range [3].

* Corresponding author: rahimpor@shirazu.ac.ir

The factors affecting the production rate in industrial methanol synthesis are parameters such as thermodynamic equilibrium limitations and catalyst deactivation, and variation in stoichiometric number. For equilibrium reactions, selective product removal or reactant addition may be used to increase conversion. Therefore, in the reaction system, the addition of CO to the reacting gas selectively leads to a shift of the chemical equilibrium towards the product side, resulting in a higher conversion of synthesis gas to methanol.

Carbon monoxide is an invisible, odorless, nonirritating, and tasteless gas that in and of itself has no (or extremely poor) sensory warning characteristics for those exposed. This fact contributes to the insidious nature of CO exposure. Carbon Monoxide is often the product of incomplete carbon-containing compounds combustion (partial oxidation).

CO is extremely toxic and causes a broad array of symptoms that precede possible death. This gas is a potential health hazard, because exposure to CO can starve critical body organs, especially the brain and heart, of oxygen. Once inside the lungs, CO molecules pass easily into the blood stream and compete with oxygen for hemoglobin (Hb) in the red blood cells. About 95% of the absorbed CO readily binds with Hb to form carboxyhemoglobin (COHb), because the affinity of Hb for CO is over 200 times stronger than it is for oxygen. Thus, the percentage of total Hb in the blood that is in the form of COHb is a biomarker of CO exposure [4, 5]. To minimize these effects, the carbon monoxide emissions from industrial sources have to be decreased. Hydrogenation of CO into methanol is today considered as one of the most promising methods to mitigate the emissions of carbon monoxide to the atmosphere. To reduce CO emissions, the development of technologies for fixing and recycling CO emissions is required. Today, one of the most promising processes for the utilization and fixation of CO is methanol synthesis. Methanol is produced by the catalytic conversion of synthesis gas (CO_2, CO and H_2) [6]. It has the advantage of being liquid under normal conditions. It can be stored and transported as easily as gasoline, and can be used in conventional combustion engines without requiring any major adjustments. Methanol has twice the energy density of liquid hydrogen and can be more conveniently stored and transported [7, 8].

Pure carbon monoxide is necessary for the enhancement of methanol synthesis in the conventional reactor with carbon monoxide injection. Three technologies that can be employed to remove and recover carbon monoxide from synthesis and other gases are pressure swing adsorption (PSA); cryogenics and absorption by a liquid (the COSORB process).

Although existing economics for CO injection in methanol synthesis are not favourable for enhancing methanol production, according to the increase in CO emission to the atmosphere from anthropogenic sources and more requests for fuels such as methanol, CO injection could be one of the ways for solving the pollution problem and enhanceing methanol production if carbon tax programs are implemented in the future.

Moreover, the water production during methanol synthesis via CO_2 hydrogenation

greatly reduced the methanol synthesis rate by suppressing the reversed water–gas shift reaction. Water produced during methanol synthesis from CO_2 conversion accelerated the crystallization of Cu and ZnO contained in a Cu/ZnO-based catalyst to lead to the deactivation of the catalyst. On the other hand, the catalyst was only slightly deactivated during methanol synthesis from a higher CO conversion, because only a small amount of water was produced during the reaction, so no remarkable crystallization of Cu and ZnO contained in the catalyst occurred [9, 10]. Therefore, one of the important key issues in most new methanol reactor configurations is that the CO-rich synthesis gas is fed to the entrance of the reactor.

Decay of catalyst activity is very common in petroleum and petrochemical industries. Unfortunately the deactivation of the catalyst in any process will force the system into unsteady operation, unless steady operation is maintained by changing the operating conditions. Therefore, dynamic behavior of the methanol reactor arises from catalyst deactivation. The transient behavior of catalyst activity can be due to many factors, such as:

- Impurities in the feed which gradually reduce active sites by physical adsorption.
- Gradual occupation of some sites by the reactants or poisons.
- Sintering

The extreme complexity of the processes involved in the methanol synthesis justify the computer simulation of such processes in order to get further understanding of the system without the need for conducting costly and time-consuming experiments. The dynamic simulation of methanol synthesis processes in particular, has a wide range of applications including; the start-up and shut-down investigations, system identification, safety, control, optimization, and transient behavior and operability studies. The dynamic simulation is preferred to steady-state simulations in operability studies since the former provides a realistic description of the transient states of the reactor owing to the fact that the numerical solution strategies employed in dynamic models are more robust than the solution of a typical steady-state model. Thus it allows for safe and trustworthy studies of the control and the optimization of the reactor [11, 12].

In literature, there are numerous studies with the aim of improving the efficiency of industrial tubular packed-bed methanol reactors. Dynamic simulation of conventional methanol synthesis reactor was investigated by Lovik et al. for long-term optimization [13]. Rahimpour et al. studied the deactivation of methanol synthesis catalyst and proposed mechanisms for deactivation of this type of catalyst [14]. Struis et al. have considered increasing the methanol yield by using a membrane reactor [15]. Rahimpour and Ghader [16, 17] investigated the Pd–Ag membrane reactors performance for methanol synthesis. They considered a steady-state homogeneous model for methanol reactor. However, there is no information available in the literature regarding the CO injection to the reactor entrance (5% CO was injected into the 95% of the feed) in the methanol synthesis reactor for the enhancement of methanol production, to mitigate the emissions of carbon monoxide

to the atmosphere. Therefore, it was decided to first study this system.

In this work, a new approach has been proposed to improve the methanol production in a fixed bed methanol synthesis reactor and to mitigate the emissions of carbon monoxide to the atmosphere by CO injection to the reactor entrance (5% CO was injected into the 95% of feed). So, a one-dimensional heterogeneous dynamic model is developed to analyze the performance of this single-type fixed-bed reactor in the presence of catalyst deactivation. The simulation results are compared with conventional methanol reactor (CMR) and membrane methanol reactor (MMR) and show that the methanol production rate in the aforesaid reactor is greater than CMR and even MMR.

2- Process description

2.1- Conventional methanol reactor (CMR)

Fig. 1 shows the scheme of a single-type methanol reactor [18]. A single-type (conventional-type) methanol reactor is basically a vertical shell and tube heat exchanger. The catalyst is packed in vertical tubes and is surrounded by boiling water. The methanol synthesis reactions are carried out over commercial $CuO/ZnO/Al_2O_3$ catalyst. The heat of the exothermic reactions is transferred to the boiling water and steam is produced. The specifications of the reactor, catalyst and feed composition are tabulated in Tables 1 and 2.

Table 1. Catalyst and specifications of CMR [18]

Parameter	Value	Parameter	Value
D_i(mm)	40.3	ε_s	0.39
D_o(mm)	44.5	ε_B	0.39
d_p(mm)	5.74	Tube side pressure (bar)	75
$a_v(m^2m^{-3})$	625.7	Tube length(m)	7.022

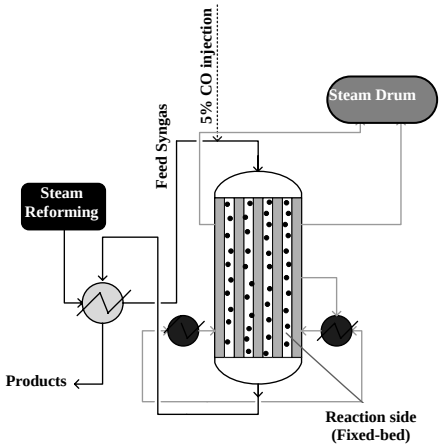

Figure 1. A schematic diagram of CMR

Table 2. Input data of the CMR [18]

Feed condition	Value
Feed composition (mole %):	
CO_2	8.49
CO	8.68
H_2	64.61
CH_4	9.47
N_2	8.2
H_2O	0.1
CH_3OH	0.37
Argon	0.24
Inlet Temperature[K]	401
Total molar flow rate per tube (mol/s)	1.8

2.2- Membrane methanol reactor (MMR)

Fig. 2 shows the schematic diagram of a membrane methanol reactor in co-current configuration. This system consists of two concentric pipes like the tube-shell system. The tubes walls in the reactor are hydrogen-permselective membrane, and the pressure difference between the shell and tube permits the diffusion of hydrogen through the Pd-based membrane layer. On the other hand, in the new system, the mass and heat transfer occurs simultaneously between the shell and tube, while in the conventional type only heat transfer occurs between them. The synthesis gas is fed to the tube side of the reactor and the high pressure product is routed from the recycle stream through the shell of the

reactor in a co-current mode with synthesis gas. The reacting gas is also cooled with the cooling saturated water which flows around it. In fact, the heat of the reaction is transferred to the cooling water and sweeping (produced) gas. After leaving the tube side of the reactor, the methanol containing gas (product) goes to the separator. The input data and catalyst specifications are the same as the CMR (see Tables 1 and 2). The specifications of the reactor are tabulated in Table 3.

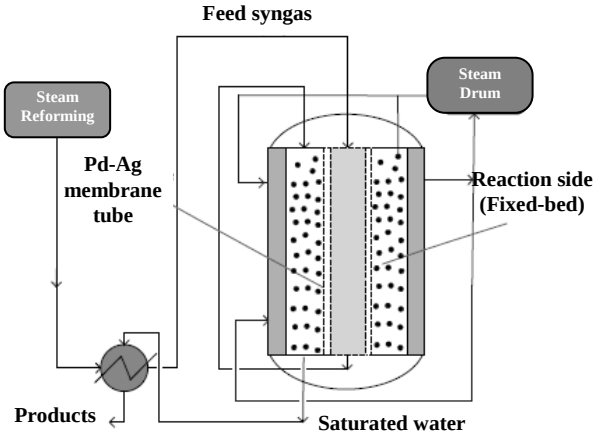

Figure 2. A schematic diagram of MMR

Table 3. Specifications of MMR

Parameter	Value	Parameter	Value
Tube diameter (m)	0.038	Tube length (m)	7.022
Shell diameter (m)	0.053	Reaction side pressure (bar)	76.98
Layer thickness (m)	8×10^{-7}	Tube side pressure (bar)	96.98

3- Mathematical modeling

3.1- Conventional methanol reactor (CMR)

Methanol reactors are traditionally modeled by a heterogeneous model, which is a conventional model for the catalytic reactor model is based on the following assumptions: (1) Ideal gas behaviour is assumed; (2) One-dimensional plug flow in the shell and tube sides; (3) Axial dispersion of heat is negligible compared to convection; (4) The radial diffusion in the catalyst pellet is neglected; (5) Reaction rates developed by Graaf et al. [19, 20] were used to obtain the main reactions rates.

The mass and energy balance for the solid phase are expressed by:

$$\varepsilon_s c_t \frac{\partial y_{is}}{\partial t} = k_{g_i} a_v . c_t . (y_i - y_{is}) + \eta r_i \rho_B a$$
$$i = 1,2,..., N-1 \quad (1)$$

$$\rho_B c_{ps} \varepsilon_s \frac{\partial T_s}{\partial t} = a_v h_f (T - T_s) + \rho_B a \sum_{i=1}^{N} \eta r_i (-\Delta H_{f,i}) \quad (2)$$

where, y_{is} and T_s are the mole fraction and temperature of the solid-phase respectively, and i represents H_2, CO_2, CO, CH_3OH, H_2O. Argon, Nitrogen and methane are inert components. The following two conservation equations are written for the fluid phase:

$$\varepsilon_B c_t \frac{\partial y_i}{\partial t} = -\frac{1}{A_c}\frac{\partial F_i}{\partial z} + a_v c_t k_{gi} (y_{is} - y_i)$$
$$i = 1,2,..., N-1 \quad (3)$$

$$\varepsilon_B c_t c_{pg} \frac{\partial T}{\partial t} = -\frac{c_{pg}}{A_c}\frac{\partial (F_t T)}{\partial z} + a_v h_f (T_s - T) + \frac{\pi D_i}{A_c} U_{shell} (T_{shell} - T) \quad (4)$$

Where, y_i and T are the fluid-phase mole fraction and temperature, respectively. The boundary conditions are known:

$$z = 0; \quad F_t = F_{in}, \quad y_i = y_{i,in}, T = T_{in} \qquad (5)$$

While the initial conditions are:

$$t = 0; \quad y_i^t = y_i^{ss}, y_{is}^t = y_{is}^{ss}, T^t = T^{ss}, T_s^t = T_s^{ss}, \ a = 1 \qquad (6)$$

3.2- Membrane methanol reactor (MMR)

The assumptions considered for the conventional methanol reactor (CMR) are also valid in the membrane methanol reactor (MMR).

3.2.1- Reaction side (Shell side)

The mass and energy balance for the solid phase in the reaction side of MMR is the same as that in the conventional methanol reactor (CMR). The following equations are written for the fluid phase:

$$\varepsilon_B c_t \frac{\partial y_i}{\partial t} = -\frac{1}{A_c}\frac{\partial F_i}{\partial z} + a_v c_t k_{gi}(y_{is} - y_i) + \frac{\alpha_H}{A_s}(\sqrt{P_H{}^t} - \sqrt{P_H{}^{sh}})$$
$$i = 1, 2, ..., N-1 \qquad (7)$$

$$\varepsilon_B c\, c_{pg}\frac{\partial T}{\partial t} = -\frac{1}{A_{shell}}C_{pg}\frac{\partial (F^{sh}T)}{\partial z} + a_v h_f (T_s - T) + \frac{\alpha_H}{A_s}(\sqrt{P_H{}^t} - \sqrt{P_H{}^{sh}})c_{ph}(T_{tube} - T) + \frac{\pi D_i}{A_{shell}}U_{tube}(T_{tube} - T) + \frac{\pi D_o}{A_{shell}}U_{shell}(T_{shell} - T) \qquad (8)$$

3.2.2- Tube side

The mass and energy balance equation for the fluid phase are given:

$$c_t \frac{\partial y_i}{\partial t} = -\frac{1}{A_c}\frac{\partial F_i^t}{\partial z} - \frac{\alpha_H}{A_c}(\sqrt{P_H{}^t} - \sqrt{P_H{}^{sh}}) \qquad (9)$$

where i denotes H_2.

$$c_t c_{pg}\frac{\partial T_{tube}}{\partial t} = -\frac{1}{A_c}C_{pg}\frac{\partial (F^t T)}{\partial z} + \frac{\alpha_H}{A_c}(\sqrt{P_H{}^t} - \sqrt{P_H{}^{sh}})C_{ph}(T - T_{tube}) + \frac{\pi D_i}{A_c}U_{tube}(T - T_{tube}) \qquad (10)$$

The boundary conditions are as follows:

$$z = 0; \quad F^t = F_{in}, \ y_i = y_{i,in}, \ T = T_{in} \qquad (11)$$

3.2.2- Hydrogen permeation through the palladium membrane

In Eqs. (7)-(10), α_H is the hydrogen permeation rate constant and is defined as [21]:

$$\alpha_H = \frac{2\pi L \bar{P}}{ln\left(\frac{R_o}{R_i}\right)} \qquad (12)$$

Where R_o and R_i stand for the outer and inner radius of the Pd–Ag layer. The permeability of hydrogen through the Pd-Ag layer as a function of temperature is as follows [22, 23]:

$$\bar{P} = P_0 exp\left(\frac{-E_p}{RT}\right) \qquad (13)$$

where the pre-exponential factor P_0 above 200°C is reported as 6.33×10^{-8} (mol/m^{2}s Pa$^{1/2}$) and activation energy E_p is 15.7 kJ/mol [22, 23].

4- Pressure drop

The Ergun momentum balance equation is used to give the pressure drop along the reactor:

$$\frac{dP}{dz} = 150\frac{(1-\varepsilon)^2 \mu u_g}{\varepsilon^3 d_p^2} + 1.75\frac{(1-\varepsilon)\rho u_g^2}{\varepsilon^3 d_p} \quad (14)$$

where the pressure drop is in Pa.

5- Reaction kinetics

Three main reactions occurring in the methanol reactor are: the hydrogenation of CO, the hydrogenation of CO_2 and the reversed water–gas shift reaction.

Kinetics of the low-pressure methanol synthesis over commercial $CuO/ZnO/Al_2O_3$ catalysts has been widely investigated. In the current study, the rate expressions have been adopted from Graaf et al [19].

The reaction rate expressions, the reaction rate constants, adsorption equilibrium constants and reaction equilibrium constants which occur in the formulation of kinetic expressions are presented in Appendix A.

6- Deactivation model

The deactivation model of the $CuO/ZnO/Al_2O_3$ catalyst has been investigated by several researchers, however the model offered by Hanken was found to be suitable for industrial applications [24]:

$$\frac{da}{dt} = -K_d \, exp\left(\frac{-E_d}{R}\left(\frac{1}{T} - \frac{1}{T_R}\right)\right) a^5 \quad (15)$$

Where, T_R, E_d and K_d are the reference temperature, activation energy and deactivation constant of the catalyst, respectively. The numerical value of T_R is 513 K, E_d is 91270 J/mol and K_d is (0.00439 h^{-1}) [24].

7- Auxiliary correlations

Auxiliary correlations should be added to solve the set of differential equations. The correlations used for the heat and mass transfer between the two phases, the physical properties of the chemical species and the overall heat transfer coefficient between the two sides are presented in Appendix B and C. The heat transfer coefficient between the gas phase and the reactor wall is applicable for the heat transfer between the gas phase and solid catalyst phase.

8- Numerical solution

The governing equations of the model form a system of coupled equations comprising algebraic, partial differential and ordinary differential equations. After rewriting the model equations at steady-state conditions, a set of differential algebraic equations (DAEs) is obtained. To solve this set of equations, backward finite difference approximation is applied here. Doing this, the DAEs change to a non-linear algebraic set of equations. The reactor is then divided into 30 separate sections and the Gauss–Newton method is used to solve the non-linear algebraic equations in each section. For the solution of the model as a function of time, the catalyst deactivation model is coupled with the model equations. To solve the system of partial differential algebraic equations of the dynamic model, different methods were tested and it was observed that the Rosenbrock method of order 2 was more efficient for such set of stiff equations.

9- Results and discussion

9.1- Steady-State model validation

The results of steady-state modeling are compared with the data reported by Harting and Keil [25]. Table 6 shows that the simulation results have a good agreement with the experimental data.

Table 4. Comparison between predicted reactor outlets with experimental data [25]

Product condition	Plant	Predicted	Error
Composition (% mole):			
CH_3OH	4.008	4.17	-4.04
CO_2	1.032	1.055	-2.18
CO	0.932	0.978	-5.02
H_2O	1.249	1.151	7.85
H_2	75.12	79.801	-6.23
N_2	3.918	4.035	-3

9.2- Model validation during the time

Model validation was also carried out by comparison of the model results with the historical process data over a period of 1200 operating days [18] under the design specifications and input data shown in Table 7. It was observed that, the model performed satisfactorily well at industrial conditions and a good agreement between the daily-observed plant data and the simulation data was obtained. Also, systematic deviation (or bias error) from the experimental values is seen owing to the fact that the kinetics used for the reaction system of methanol synthesis underestimates the true reaction rates.

9.3- Effect of CO injection on mole fraction of components and temperature profiles

Fig. 2(a) shows the methanol mole fraction along the conventional methanol reactor (CMR) without injection, MMR and CMR with 5% CO injection to the 95% of the conventional feed. As shown in this figure, the methanol mole fraction is higher, while 5% CO is injected to the entrance of CMR in comparison with other cases. Moreover, in the case of 5% CO injection to CMR, more hydrogen is consumed and converted to methanol as can be seen in Fig. 2(b). Also, in Fig. 2(c) the H_2O mole fraction along the reactor shows that when CO is injected to the reactor, the water gas shift (WGS) reaction moves in the water consumption direction and this caused more hydrogen to be produced in CMR, so more methanol was produced in the case of CO injection. This is one of the advantages of CO injection to a system of single-type configuration.

Gas phase temperature versus the reactor length was investigated in Fig. 2(d). CO injection leads to making a higher temperature along the reactor. By injecting CO to a single-type configuration, and increasing CO concentration as the reactant component, according to WGS reaction, more hydrogen is produced in the reaction side, therefore a higher reactants concentration is observed in the case of CO injection and thus more reaction heat is released. This is the reason why the gas temperature increases in the CO injection manner.

Table 5. Comparison between predicted methanol production rates with plant data [18]

Time(Day)	Plant(ton/day)	Predict(ton/day)	Error	Time(Day)	Plant(ton/day)	Predict(ton/day)	Error
0	295	310.4	-5.22	700	274	268.7	1.93
100	296.5	297.5	-0.34	800	268.1	265.9	0.82
200	302.6	289.7	4.26	900	275.5	263.4	4.39
300	284.3	283.9	0.14	1000	274.6	261.1	4.91
400	277.9	279.1	-0.04	1100	262.2	258.9	1.52
500	278.2	275.2	1.08	1200	255.2	257	-0.71
600	253	271.7	-7.39				

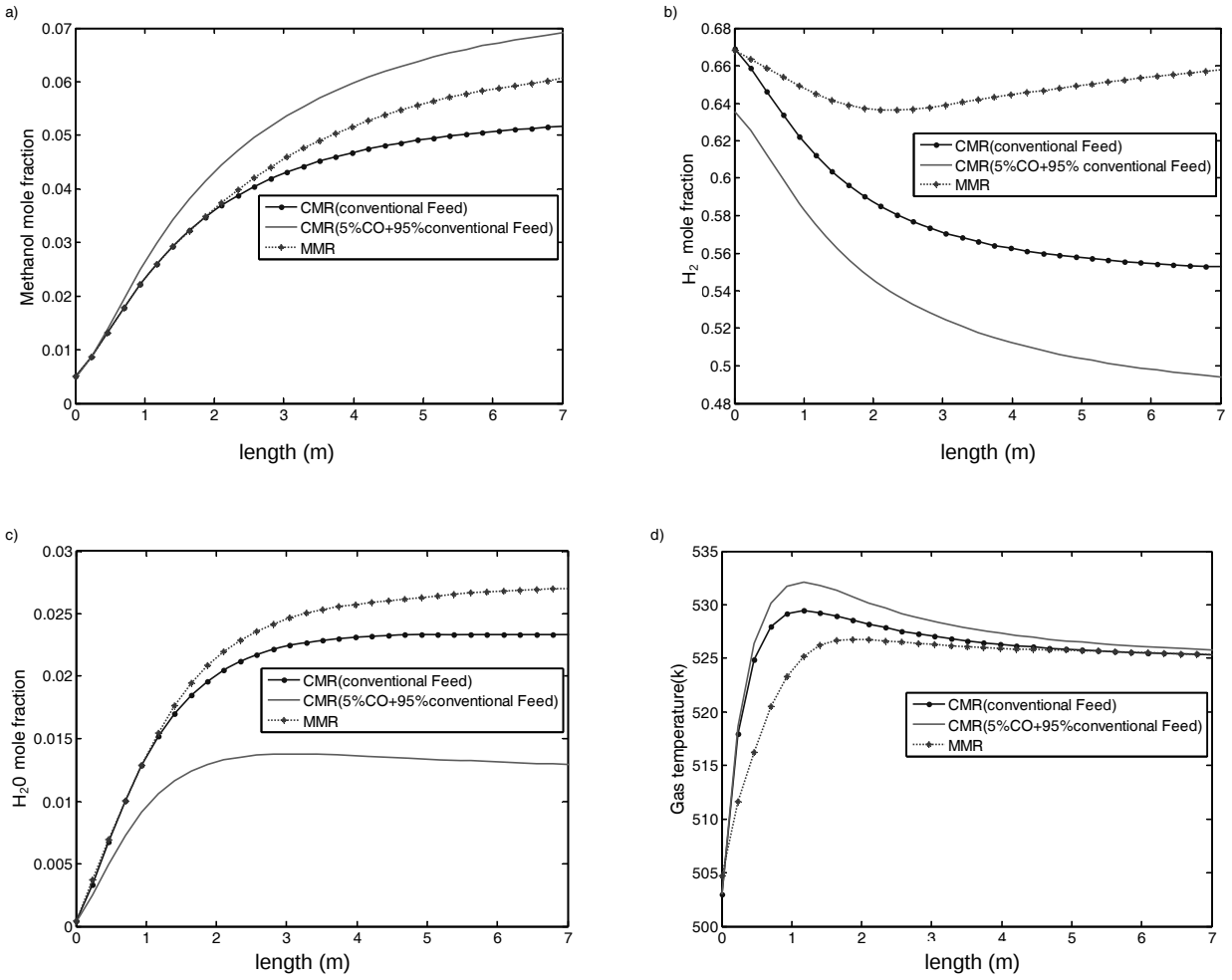

Figure 3. Comparison between (a) CH_3OH mole fraction, (b) H_2 mole fraction, (c) H_2O mole fraction and (d) gas temperature in the cases of the CMR (conventional feed), CMR (5% CO injection to 95% of conventional feed) and MMR for fresh catalyst

9.4- Results of dynamic simulation

Dynamic simulation is carried out to address vital issues such as the reacting gas temperature, methanol mole fraction, CO mole fraction, H_2 mole fraction and catalyst activity as a function of time and the length of the reactor, while 5 percent of CO was injected to the entrance of the CMR. Fig. 3(a) shows the reacting gas temperature as a function of the time and length of the reactor. At initial times, the temperature of the catalyst bed cannot be controlled around the hot spot; whereas, as the catalyst deactivates, the peak of the temperature in the hot spot subsides so that at the end of the duration there is no sign of a hot spot. It is due to this fact that, as time goes on the catalyst deactivates and heat dissipation by reaction is decreased so that the water coolant could remove the heat of the reaction.

Fig. 3(b) shows the profile of methanol mole fraction along the reactor as time goes on. This profile is similar to steady-state simulation where the methanol mole fraction

increases along the reactor, although the rate of conversion decreases. Catalyst deactivation is the main reason for the reduction in the methanol mole fraction as time goes on. The deactivation dynamic pattern of the catalyst along the reactor is shown in Fig. 3(c). There is an extremely sharp rate of deactivation in a small fraction of the process time, which is followed by a relatively slow deactivation rate for the reminder of the process time. As shown over 200 days of operation, the catalyst activity decreases from approximately 1 to 0.6. Also, it is seen that after a conventional process time, the activity of the catalyst is equal to 0.38.

Also, in Fig. 4 the reactants mole fractions are plotted as a function of length and time. As it can be seen, reactants mole fractions decreased along the reactor length, but this comparison in the case of time represent that when time passed, the CO and H_2 mole fraction increased because of the catalyst deactivation and less reactant was converted to production.

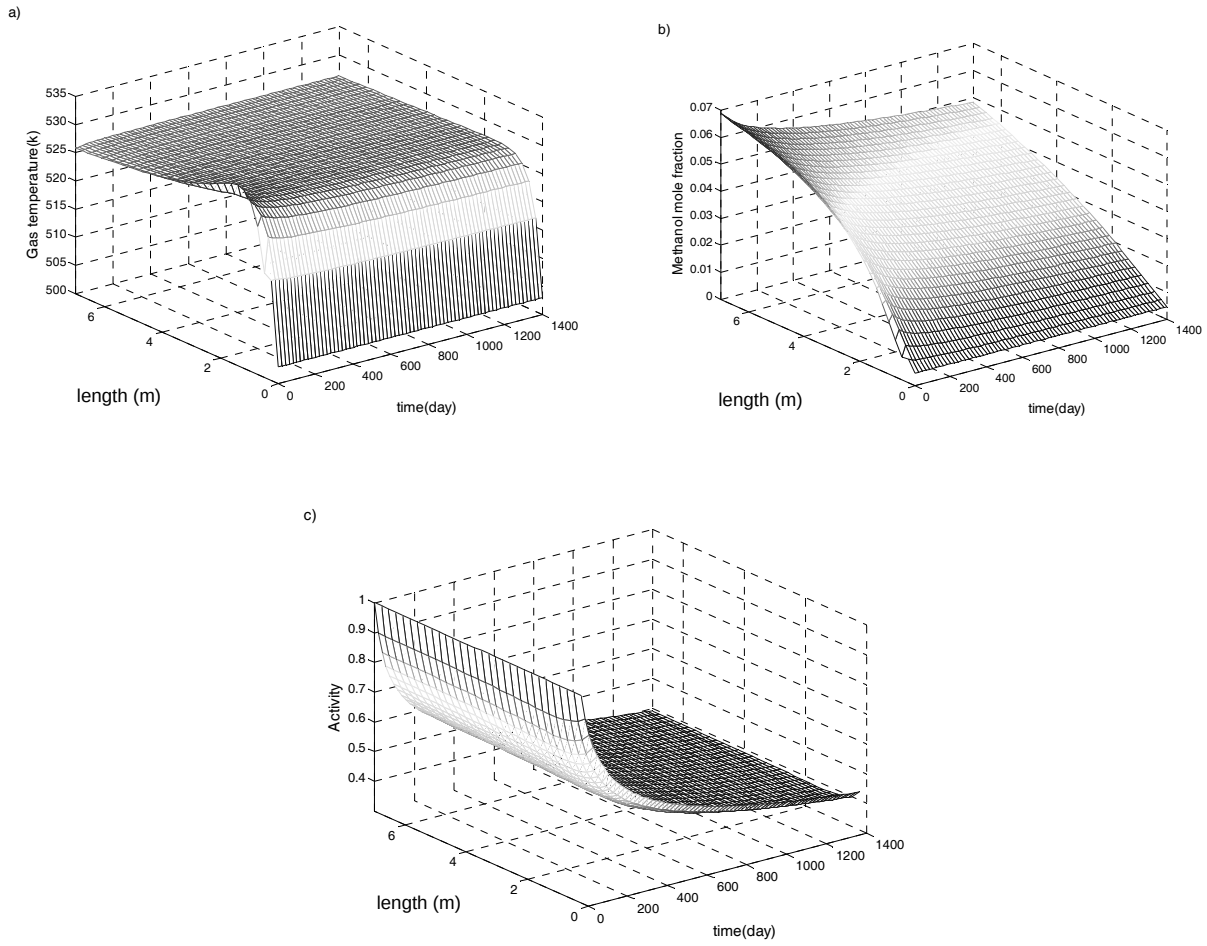

Figure 4. Profiles of (a) temperature gas (b) methanol mole fraction and (c) activity along the reactor and time for CMR (5% CO injection to 95% of conventional feed)

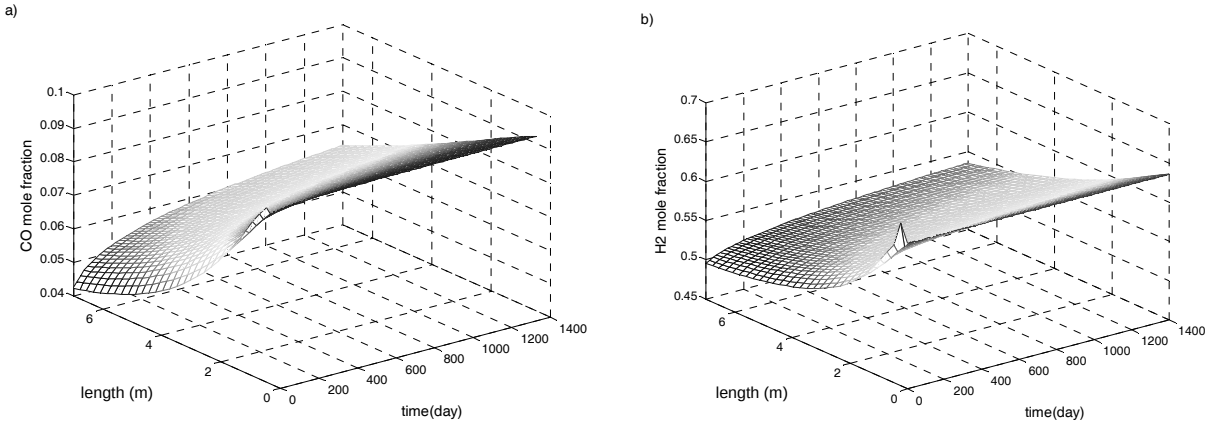

Figure 5. Profiles of (a) CO mole fraction and (b) H_2 mole fraction along the reactor and time for CMR (5% CO injection to 95% of conventional feed)

In Fig. 5 a comparison between three types of single-type reactor such as a conventional single-type of methanol reactor (CMR), membrane single-type methanol reactor (MMR) and conventional single-type reactor with 5% CO injection to the entrance of the reactor was shown. At first, in Fig. 5(a) the average of the methanol mole fraction over a period of 1400 operating days for the aforesaid reactor cases was investigated. As we can see in this figure, in the case of the CMR with 5% CO injection to the entrance of the reactor, more methanol is produced in contrast with the two other cases in this operating period. In another figure the average of the water mole fraction over a period of 1400 operating days was plotted for three types of reactor configurations. In this figure, for a membrane single-type reactor more water is produced in this operating period because when membrane is applied in a single-type configuration, hydrogen penetration caused the WGS reaction to move to water production. This is a big disadvantage for methanol catalysts because the higher water production rate increases catalyst re-crystallization. So it is obvious that in the case of CO injection to CMR, a higher methanol mole fraction can be achieved without having to apply expensive processes such as adding membrane, and by using this procedure the catalyst is in safe mode because of the low water production. Injecting CO leads the WGS reaction to move in water consumption and fewer sights of catalyst ruined by water. This mode can improve the catalyst lifetime. Overall, the most important point in this study is using a membrane in the methanol single-type reactor is an expensive way for increasing the methanol production rate and this way has a great disadvantage which our catalysts deactivate rapidly by more water production, but, on the other hand, injecting CO is a better way, from an economic aspect, to increase methanol production with lower water production.

In other plots, the average of the reactants

mole fraction over a period of 1400 operating days for the three modes of reactors was demonstrated. It is quite obvious that more CO exists in our reactor system, but in the membrane single-type system, because of hydrogen permeation through the membrane and CO consumption, moving the WGS reaction to CO production is higher in comparison with the one without membrane. But in the other figure, the average of the hydrogen mole fraction was investigated for three modes of reactor configuration. In CMR, with 5% CO injection to the entrance of the reactor, owing to moving WGS to hydrogen caused hydrogen consumption to be higher with other aspects of other reactors configurations.

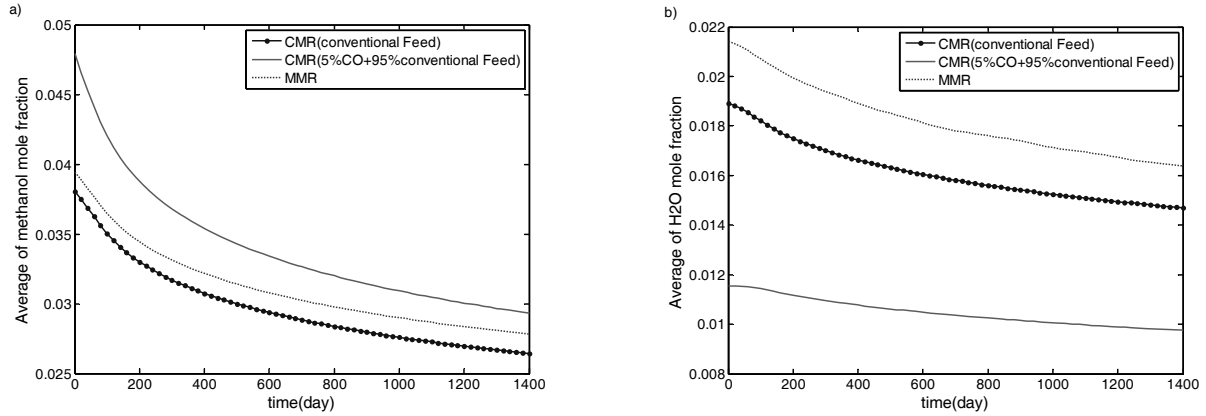

Figure 6. Comparison between (a) average of methanol mole fraction and (b) average of H_2O mole fraction over a period of 1400 days of operation for CMR (conventional feed), CMR (5% CO injection to 95% of conventional feed) and MMR systems

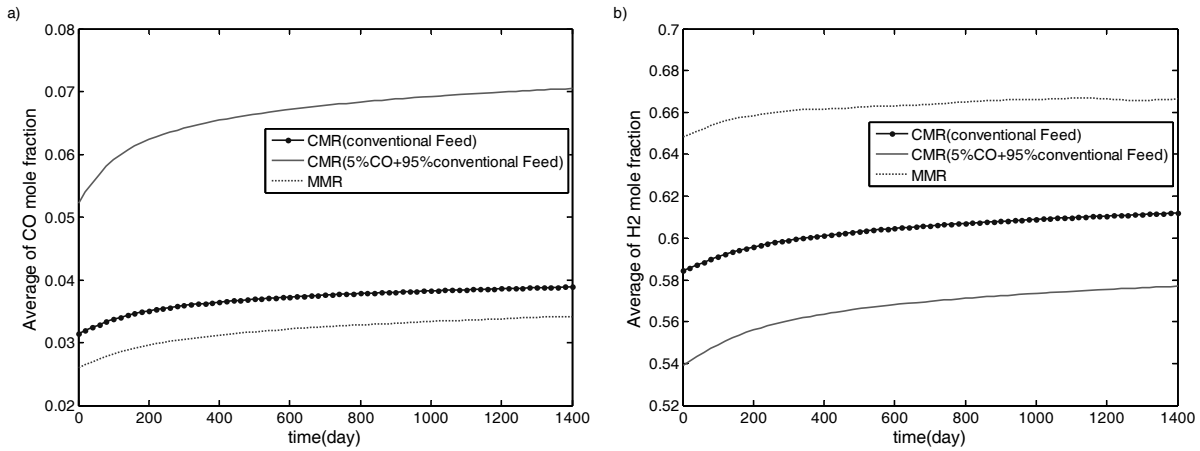

Figure 7. Comparison between (a) average of CO mole fraction and (b) average of H_2 mole fraction over a period of 1400 days of operation for CMR (conventional feed), CMR (5% CO injection to 95% of conventional feed) and MMR systems

A comparison of the methanol production rate in the three types of reactors at the first day, 1400th day and over a period of 1400 days of operation as the average are presented in Fig. (7). As can be seen, there is a considerable increase in the amount of methanol production in a conventional reactor with 5% CO injection.

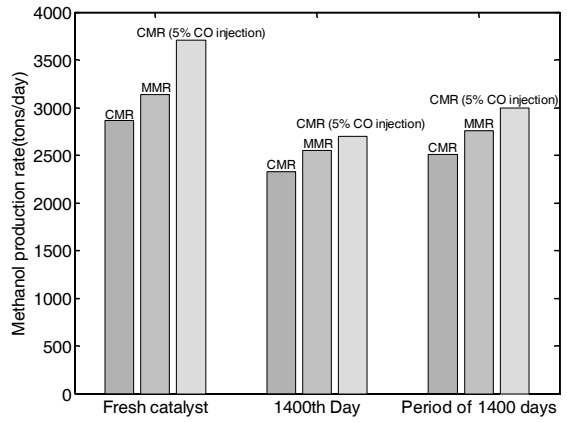

Figure 8. Comparison of methanol production in three types of reactor

10- Conclusions

The CO injection analysis of the single fixed bed methanol reactor shows a 14.24% and 22.93% enhancement in the yield of methanol production in comparison with MMR and CMR, respectively, while 5% CO was injected into the 95% of the feed. Also, by CO injection to the feed, water produced during methanol synthesis via CO_2 hydrogenation, which accelerates the catalyst deactivation and reduces the methanol production rate, is considerably reduced. On the other hand, CO is an important cause of pollution and a hazardous material in many industrial processes which must be removed and this method is a suitable method for this case.

11- Appendix

11.1- Appendix A. Reaction kinetics

In the conversion of synthesis gas to methanol, three overall reactions are possible: hydrogenation of carbon monoxide, hydrogenation of carbon dioxide and reverse water-gas shift reaction, which follow as:

$$CO + 2H_2 \leftrightarrow CH_3OH$$
$$\Delta H_{298} = -90.55 \ \frac{kJ}{mol} \qquad \text{(A-1)}$$

$$CO_2 + H_2 \leftrightarrow CO + H_2O$$
$$\Delta H_{298} = +41.12 \ \frac{kJ}{mol} \qquad \text{(A-2)}$$

$$CO_2 + 3H_2 \leftrightarrow CH_3OH + H_2O$$
$$\Delta H_{298} = -49.43 \ \frac{kJ}{mol} \qquad \text{(A-3)}$$

Reactions (A-1) to (A-3) are not independent so that one is a linear combination of the others. In the current work, the rate expressions have been selected from Graaf et al. [19]. The rate equations combined with the equilibrium rate constants [20] provide enough information regarding the kinetics of methanol synthesis. The correspondent rate expressions, due to the hydrogenation of CO, CO_2 and the reversed water-gas shift reactions are:

$$r_1 = \frac{k_1 K_{CO}[f_{CO} {f_{H_2}}^{3/2} - f_{CH3OH}/({f_{H2}}^{1/2} K_{P1})]}{(1 + K_{CO} f_{CO} + K_{CO_2} f_{CO_2})[{f_{H_2}}^{1/2} + (K_{H_2O}/{K_{H_2}}^{1/2}) f_{H_2O}]} \qquad \text{(A-4)}$$

$$r_2 = \frac{k_3 K_{CO_2}[f_{CO_2} f_{H_2} - f_{H_2O} f_{CO}/K_{P3}]}{(1 + K_{CO} f_{CO} + K_{CO_2} f_{CO_2})[{f_{H_2}}^{1/2} + (K_{H_2O}/{K_{H_2}}^{1/2}) f_{H_2O}]} \qquad \text{(A-5)}$$

$$r_3 = \frac{k_2 K_{CO_2}[f_{CO_2} f_{H_2}{}^{3/2} - f_{CH_3OH} f_{H_2O}/(f_{H_2}{}^{3/2} K_{p2})]}{(1 + K_{CO} f_{CO} + K_{CO_2} f_{CO_2})[f_{H_2}{}^{1/2} + (K_{H_2O}/K_{H_2}{}^{1/2}) f_{H_2O}]} \quad \text{(A-6)}$$

The reaction rate constants, adsorption equilibrium constants and reaction equilibrium constants which occur in the formulation of kinetic expressions are tabulated in Tables A-1 through A-3, respectively.

Table A-1. Reaction rate constants [20].

$k = A\exp(\frac{B}{RT})$	A	B
K_1	$(4.89\pm0.29)\times 10^7$	-113000±300
K_2	$(9.64\pm7.30)\times 10^7$	-152900±11800
K_3	$(1.09\pm0.07)\times 10^7$	-87500±300

Table A-2. Adsorption equilibrium constants [20].

$k = A\exp(\frac{B}{RT})$	A	B
K_{CO}	$(2.16\pm0.44)\times 10^{-5}$	46800±800
K_{CO2}	$(7.05\pm1.39)\times 10^{-7}$	61700±800
$(K_{H2O}/K_{H2}{}^{1/2})$	$(6.37\pm2.88)\times 10^{-9}$	84000±1400

Table A-3. Reaction equilibrium constants [20].

$k = A\exp(\frac{B}{RT})$	A	B
K_{p1}	5139	12.621
K_{P2}	-2073	-2.029
K_{P3}	3066	10.592

11.2- Appendix B. Auxiliary correlations

B.1. Mass transfer correlations

In the current work, mass transfer coefficients for the components have been taken from Cusler [26]. These are mass transfer coefficients between the gas and the solid phase.

$$k_{gi} = 1.17\, Re^{-0.42} Sc_i{}^{-0.67} u_g .10^3 \quad \text{(B-1)}$$

where the Reynolds and Schmidt numbers have been defined as:

$$Re = \frac{2R_p u_g}{\mu} \quad \text{(B-2)}$$

$$Sc_i = \frac{\mu}{\rho\, D^i{}_m .10^{-4}} \quad \text{(B-3)}$$

and the diffusivity of component i in the gas mixture is given by [27].

$$D_{im} = \frac{1 - y_i}{\sum_{i=j} \frac{y_i}{D_{ij}}} \quad \text{(B-4)}$$

And also, the binary diffusivities are calculated using the Fuller-Schetter-Giddins equation reported by Reid and his co-workers [28]. In the following Fuller-Schetter-Giddins correlation, vci, Mi are the critical volume and molecular weight of component i which are reported in Table B.1 [29].

$$D_{ij} = \frac{10^{-7} T^{3/2} \sqrt{\frac{1}{M_i} + \frac{1}{M_j}}}{P(v_{ci}{}^{3/2} + v_{cj}{}^{3/2})^2} \quad \text{(B-5)}$$

Knowing the fact that diffusion path length along the pores is greater than the measurable thickness of the pellet, for the effective diffusivity in the catalyst pore, the correction should be implemented due to the structure of the catalyst. The correction factor is the ratio of the catalyst void fraction to the tortuosity of the catalyst (τ).

Table B.1. Molecular weight and critical volume of the components

Component	M_i (g/mol)	vci (m_3/mol)×10^6
CH_3OH	32.04	118.0
CO_2	44.01	94.0
CO	28.01	18.0
H_2O	18.02	56.0
H_2	2.02	6.1
CH_4	16.04	99.0
N_2	28.01	18.5

B.2- Heat transfer correlations

The overall heat transfer coefficient between the circulating boiling water of the shell side and the bulk of the gas phase in the tube side is given by the following correlation.

$$\frac{1}{U_{shell}} = \frac{1}{h_i} + \frac{A_i \, ln(\frac{D_o}{D_i})}{2\pi L K_w} + \frac{A_i}{A_o}\frac{1}{h_o} \qquad \text{(B-6)}$$

where, hi is the heat transfer coefficient between the gas phase and the reactor wall and is obtained by the following correlation [30].

$$\frac{h_i}{C_p \rho \mu}\left(\frac{C_p \mu}{K}\right)^{2/3} = \frac{0.458}{\varepsilon_B}\left(\frac{\rho u d_p}{\mu}\right)^{-0.407} \qquad \text{(B-7)}$$

where, in the above equation, u is the superficial velocity of gas and the other parameters are those of the bulk gas phase and d_p is the equivalent catalyst diameter, K is the thermal conductivity of gas, ρ, μ are the density and viscosity of gas, respectively and εB is the void fraction of the catalyst bed.

In equation B-6, ho is the heat transfer coefficient of boiling water in the shell side, estimated by the following equation [31].

$$h_o = 7.96(T - T_{sat})^3 (\frac{P}{P_a})^{0.4} \qquad \text{(B-8)}$$

T and P are the temperature and pressure of boiling water in the shell side, T_{sat} is the saturated temperature of boiling water at the operating pressure of the shell side and P_a is the atmospheric pressure. The last term of the above equation has been considered due to the effect of pressure on the boiling heat transfer coefficient. For the heat transfer coefficient between the bulk gas phase and the solid phase (h_f), Eq. (B-10) is applicable.

11.3- Appendix C. Dusty gas model

It is said that commercial size $CuO/ZnO/Al_2O_3$ catalysts exhibit intra-particle diffusion limitations, so in the modeling of an industrial fixed-bed methanol synthesis process, internal mass transport limitation should be taken into account. Dusty gas model is widely used to describe intra-particle diffusion limitations in methanol synthesis over commercial $CuO/ZnO/Al_2O_3$ catalysts.

When reactants diffuse into the pores to react and form products and bulk, Knudsen and surface diffusions may take place simultaneously, depending on the size of the pores, the molecules involved in the diffusing stream, the operating conditions and the geometry of the pores. In the dusty gas model which is based on Stefan-Maxwell equations, both diffusional and convective mass transport terms are considered, and this includes the description of pressure drop over the catalyst particle resulting from the

stoichiometry of the reaction and the accompanying convective transport of molecules. The results of sensitivity analysis show that at low pressures (up to 10 bar), Knudsen diffusion is the most important diffusing term; while at high pressures (100 bar) bulk diffusion predominates.

In this model, it is assumed that pore walls consist of giant molecules ('dust') which are uniformly distributed in the space. These dust molecules are considered to be dummy, or pseudo species in the mixture.

The dusty gas flux relations can be offered as follows, with a small change in the notation as to avoid conflicting with other notations used in the model:

$$\frac{N_i}{D_i^{Eff}} + \sum_{i \neq j}^{N} \left(\frac{y_j N_i - y_i N_j}{D_{ij}^{Eff}} \right) = -\frac{P}{RT}\frac{dy_i}{dr} - \frac{y_i}{RT}\left(1 + \frac{B_0 P}{\mu D_i^{Eff}}\right)\frac{dP}{dr} \qquad \text{(C.1)}$$

In the above equation, B_0 is permeability of the catalyst pellet, D_i^{Eff} is the effective Knudsen diffusion coefficient and D_{ij}^{Eff} is the effective binary diffusion coefficient which is presented by equation C.2 and C.3 below, respectively:

$$D_i^{Eff} = a_p \frac{\varepsilon_s}{\tau}\frac{2}{3}\left[\frac{8RT}{\pi M_i}\right]^{1/2} \qquad \text{(C.2)}$$

$$D_{ij}^{Eff} = \frac{\varepsilon_s}{\tau} D_{ij} \qquad \text{(C.3)}$$

where, a_p is the mean pore radius.

The dusty gas flux relations (Eqs. C.1 through C.3) contain three parameters: the mean pore radius, a, the ration of porosity and tortuosity factors, εs/τ and the permeability parameter, B_0. Using darcy's law, combining the two parameters of permeability and the mean pore radius gives a two-parameter model using the following correlation:

$$B_0 = \frac{{a_p}^2}{8} \qquad \text{(C.4)}$$

The reader should note that the flux relations (Eq. C.1) could be rewritten for distinct components to form a set of ordinary differential equations, yielding expressions for $\frac{dy_i}{dr}$. Knowing the fact that the summation of all components equals 1 (i.e., $\sum_1^N y_i = 1$), N-1 ordinary differential equations should be written for the flux relations.

To complete the mathematical modeling of the dusty gas model, the material balances and the stoichiometric relations have to be added in order to be able to describe the multicomponent reaction-diffusion problem. Since we have used the detailed Graaf kinetics for the system of methanol synthesis process, which is based on three-independent reactions, it is necessary to add three material balances to the flux relations. For a spherical and isothermal particle, this yields:

$$\frac{d\Omega_k}{dr} = r^2 r_k = \qquad \text{k=1, 2, 3} \qquad \text{(C.5)}$$

$$\frac{dy_i}{dr} = -\frac{1}{r^2}\left(\sum_{k=1}^{3}\Omega_k \sum_{j=1}^{5} \nu_{kj} F_{ij}\right)$$

(i=1, 2, …, N-1) (C.6)

$$F_{ii} = \frac{RT}{P}\left(\frac{1}{D_i^{Eff}} + \sum_{\substack{j=1 \\ j\neq i}}^{5}\frac{y_i}{D_{ij}^{Eff}} - \frac{y_i}{D_i^{Eff}}\left(1+\frac{B_0 P}{\mu D_i^{Eff}}\right)\frac{1}{w}\right) \quad (C.7)$$

$$F_{ij} = -\frac{RT}{P}\left(\frac{y_i}{D_{ij}^{Eff}} + \frac{y_i}{D_j^{Eff}}\left(1+\frac{B_0 P}{\mu D_i^{Eff}}\right)\frac{1}{w}\right) \quad (C.8)$$

$$w = 1+\frac{B_0 P}{\mu}\sum_{i=1}^{N}\frac{y_i}{D_i^{Eff}} \quad (C.9)$$

Where, F_{ii}, F_{ij}, w and Ω_k are auxiliary parameters and v is the stoichiometric coefficient

The pressure drop in the radial coordinate is given by:

$$\frac{dP}{dr} = -\frac{1}{r^2}\frac{RT}{w}\sum_{i=1}^{N}\left(\frac{1}{D_i^{Eff}}\sum_{k=1}^{3}\nu_{ik}\Omega_k\right) \quad (C.10)$$

The boundary conditions for the set of ordinary differential equations are given by:

$$\Omega_k = 0 \quad (k=1,2,3) \quad at \quad r=0 \quad (C.11)$$

$$y_i = y_{is} \quad (i=1,2,3,4) \quad at \quad r=R_p \quad (C.12)$$

$$P = P^s \quad at \quad r=R_p \quad (C.13)$$

The effectiveness factors for methanol and water would be obtained, as the following correlations are based on equation C.5 and the fact that methanol is produced via reactions (A.1) and (A.2), while water is produced via reactions (A.2) and (A.3) .

$$\eta_{CH_3OH} = \frac{3}{R_p^3}\frac{\left(\Omega_1^s+\Omega_2^s\right)}{r_1^s+r_2^s} \quad (C.14)$$

$$\eta_{H_2O} = \frac{3}{R_p^3}\frac{\left(\Omega_2^s+\Omega_3^s\right)}{r_2^s+r_3^s} \quad (C.15)$$

Where, superscript s means that the variable has been calculated at the surface of the catalyst pellet.

12- Nomenclature

Symbol	Unit	Definition
A_c	m^2	cross section area of each tube
A_{shell}	m^2	cross section area of shell
a	[-]	Activity
a_v	$m^2.m^{-3}$	specific surface area of catalyst pellet
c_{Pg}	$J.mol^{-1}.k^{-1}$	specific heat of the gas at constant pressure
c_{Ps}	$J.mol^{-1}.k^{-1}$	specific heat of the catalyst at constant pressure
c_t	$mol.m^{-3}$	total concentration

D	m	Reactor diameter
D_i	m	tube inside diameter
D_o	m	tube outside diameter
d_p	m	particle diameter
E_d	$J.mol^{-1}$	activation energy used in the deactivation model
F_t	$mole.s^{-1}$	total molar flow per tube
f_i	bar	partial fugacity of component i
h_f	$W.m^{-2}.K^{-1}$	gas-catalyst heat transfer coefficient
K	$W.m^{-1}.K^{-1}$	conductivity of fluid phase
K_d	s^{-1}	deactivation model parameter constant
K_i	bar^{-1}	adsorption equilibrium constant for component i
K_{Pi}	[-]	equilibrium constant based on partial pressure for component i
k_1	$mol.kg^{-1}.s^{-1}.bar^{-1/2}$	reaction rate constant for the 1st rate equation
k_2	$mol.kg^{-1}.s^{-1}.bar^{-1/2}$	reaction rate constant for the 2nd rate equation
k_3	$mol.kg^{-1}.s^{-1}.bar^{-1/2}$	reaction rate constant for the 3rd rate equation
k_{gi}	$m.s^{-1}$	mass transfer coefficient for component i
L	m	length of reactor
M_i	$g.mol^{-1}$	molecular weight of component i
N	[-]	number of components
P	bar	total pressure
R	$J.mol^{-1}.K^{-1}$	universal gas constant
r_i	$mol.kg^{-1}.s^{-1}$	reaction rate of component i
r_1	$mol.kg^{-1}.s^{-1}$	rate of reaction for hydrogenation of CO
r_2	$mol.kg^{-1}.s^{-1}$	rate of reaction for hydrogenation of CO_2
r_3	$mol.kg^{-1}.s^{-1}$	reversed water-gas shift reaction
T	K	bulk gas phase temperature
T_s	K	temperature of solid phase
T_{sat}	K	saturated temperature of boiling water at operating pressure
T_{shell}	K	temperature of coolant stream, in the first reactor
T_{tube}	K	temperature of coolant stream, in the second reactor
t	s	Time
U_{shell}	$W.m^{-2}.K^{-1}$	overall heat transfer coefficient between coolant and process streams
U	$m.s^{-1}$	superficial velocity of fluid phase
y_i	[-]	mole fraction of component i in the fluid phase
y_{is}	[-]	mole fraction of component i in the solid phase
z	m	axial reactor coordinate

Greek letters

Symbol	Unit	Definition
$\Delta H_{f,i}$	J.mol^{-1}	enthalpy of formation of component i
ΔH_{298}	J.mol^{-1}	enthalpy of reaction at 298 °K
ε_B	[-]	void fraction of catalytic bed
ε_s	[-]	void fraction of catalyst
ν	[-]	stoichiometric coefficient
ρ_B	kg.m^{-3}	density of catalytic bed
η	[-]	catalyst effectiveness factor

Superscripts and subscripts

i	component *i*
f	feed conditions
in	inlet conditions
out	outlet conditions
k	reaction number index (1, 2 or 3)
s	catalyst surface
sh	shell side
ss	initial conditions (i.e., steady-state condition)
t	Tube side

References

[1] Semelsberger, T. A., Borup, R. L., and Greene, H. L., "Dimethyl ether (DME) as an alternative fuel", *J. Power Sources*, 156 (2), 497 (2006).

[2] Chinchen, G. C., Denny, P. J., Jennings, J. R., Spencer, M. S. and Waugh, K. C., "Synthesis of methanol: Part 1: Catalysts and Kinetics", *Appl. Catal*., 36, 1 (1988).

[3] Schack, C. J., Mcneil, M. A., and Rinker, R. G., "Methanol synthesis from hydrogen, carbon monoxide and carbon dioxide over a Cuo/ZnO/Al_2O_3 catalyst. i. steady-state kinetics experiments", *Appl. Catal.,* 50, 247 (1989).

[4] Chung, Y., Park, S. E., Lee, K., Yanagisawa, Y. and Spengler, J. D., "Determinations of personal carbon monoxide exposure and blood carboxyhemoglobin", Yonsei Medical Journal, 35 (4), 420 (1994).

[5] Penney, D.G., Carbon monoxide poisoning, CRC Press, Taylor & Francis Group, Boca Raton London, New York, pp. 198-199 (2008).

[6] Eliasson, B., Carbon Dioxide Chemistry: Environmental Issues*,* Cambridge, in Paul, J., and Pradier, C. M. (eds.), The Royal Society of Chemistry, pp. 5-15 (1994).

[7] Gallucci, F., Basile, A., and Drioli, E., "Methanol as an energy source and/or energy carrier in membrane processes", *Sep. Purif. Rev*., 36 (2), 175 (2007).

[8] Highfield, J. G., Bill, A., Eliasson, B., Geiger, F., and Uenala, E., "The role of simple alcohols in renewable hydrogen energy cycles", *11th Int. Symp. Alcohol Fuels (ISAF XI),* Sun City, South Africa, (1996).

[9] Wu, J., Saito, M., Takeuchi, M. and Watanabe, T., "The stability of Cu/ZnO-based catalysts in methanol synthesis from a CO_2-rich feed and from a CO-rich feed", *Appl. Catal. A*, 218, 235 (2001).

[10] Rahimpour, M. R., Fathikalajahi, J., and Jahanmiri. A., "Selective kinetic deactivation model for methanol synthesis from simultaneous reaction of CO_2 and CO with H_2 on a commercial copper/zinc oxide catalyst", *Can. J. Chem. Eng.*, 76, 753 (1998).

[11] Vasco de Toledo, E. C., de Santana, P. L., WolfMaciel, M. R., and Filho, R. M., "Dynamic modeling of a three-phase catalytic slurry reactor", *Chem. Eng. Sci.,* 56, 6055, (2001).

[12] Setinca, and Levecb, J., "Dynamics of a mixed slurry reactor for the three phase methanol synthesis", *Chem. Eng. Sci.*, 56, 6081, (2001).

[13] Lovik, I., Hillestad, M., and Hertzberg, T., "Long Term Dynamic Optimization of a Catalytic Reactor System", *Comput. Chem. Eng*., 22, 707, (1998).

[14] Rahimpour, M. R., Fathikalajahi, J., and Jahanmiri, A., "Selective kinetic deactivation model for methanol synthesis from simultaneous reaction of CO_2 and CO with H_2 on a commercial copper/zinc oxide catalyst", *Can. J. Chem. Eng*., 76, (1998).

[15] Struis, R. P. W. J., Stucki, S., and Wiedorn, M., "A membrane reactor for methanol synthesis", *J. Membrane Sci*., 113, 93, (1996).

[16] Rahimpour, M. R., and Ghader, S., "Theoretical Investigation of a Pd-Membrane Reactor for Methanol Synthesis", *Chem. Eng. Technol.,* 26 (8), 902, (2003).

[17] Rahimpour, M. R., and Ghader, S., "Enhancement of CO conversion in a novel Pd–Ag membrane reactor for methanol synthesis", *Chem. Eng. Process*, 43 (9), 1181, (2004).

[18] Domestic Petrochemical Complex, "Operating data sheets of methanol plant", (2000–2003).

[19] Graaf, G. H., Stamhuis, E. J., and Beenackers, A. A. C. M., "Kinetics of low-pressure methanol synthesis", *Chem. Eng. Sci*., 43 (12), 3185, (1988).

[20] Graaf, G. H., Sijtsema, P. J. J. M., Stamhuis, E. J., and Joosten, G. E., "Chemical equilibrium in methanol synthesis", *Chem. Eng. Sci*., 41 (11), 2883, (1986).

[21] Hara, S., Xu, W. C., Sakaki, K., and Itoh, N., "Kinetics and hydrogen removal effect for methanol decomposition", *Ind. Eng. Chem. Res.*, 38 (2), 488, (1999).

[22] Barbieri, G., and Maio, F. P. D., "Simulation of the methane steam re-forming process in a catalytic Pd-membrane reactor", *Ind. Eng. Chem. Res*., 36 (6), 2121, (1999).

[23] Shu, G., Grandjean, B. P. I., and Kaliaguine, S., "Methane steam reforming in symmetric Pd– and Pd–Ag / porous ss membrane reactor", *Appl. Catal., A*, 119 (2), 305, (1994).

[24] Hanken, L., "Optimization of methanol reactor: Master's Thesis", *The Norwegian University of Science and Technology,* (1995).

[25] Harting, F., and Keil, F. J., "Large-scale spherical fixed bed reactors: modeling and optimization", *J. Ind. Eng. Chem. Res*., 32, 424, (1993).

[26] Cussler, E. L., Diffusion–mass transfer in fluid *systems*, Cambridge University Press, Cambridge, (1984).

[27] Wilke, C. R., "Estimation of Liquid diffusion coefficients", *Chem. Eng. Prog.*, 45, 218, (1949).

[28] Reid, R. C., Sherwood, T. K., and Prausnitz, J., The properties of gases and liquids, 3rd ed., McGraw-Hill, New York, (1977).

[29] Hartig, F., and Keil, F. J., "Large-scale spherical fixed bed reactors: modeling and optimization", *Ind. Eng. Chem. Res.*, 32 (3), 424, (1993).

[30] Smith, J. M., Chemical engineering kinetics, McGraw-Hill, New York, (1980).

[31] Holman, J. P., Heat transfer, McGraw-Hill, New York, (1989).